Proceedings World Geothermal Congress 2020+1
Reykjavik, Iceland, April - October 2021

Geo-electrical Monitoring of H2S Mineralization into Pyrite, upon Re-injection in Basalts at Nesjavellir Geothermal site, Iceland

Léa Lévy[1,2], Pradip K. Maurya[2], Gianluca Fiandaca[3], Thue S. Bording[2], Line M. Madsen[2], Lydie Gailler[4], Svetlana Byrdina[5], Thomas Ratouis[6], Sigrún Tómasdóttir[6], Bergur Sigfússon[7], Knútur Árnason[1]

[1]ÍSOR, Iceland GeoSurvey, Grensásvegur 9, 108 Reykjavik, Iceland

lea@isor.is

[2]HydroGeophysics Group, Department of Geoscience, Aarhus University, Denmark

[3]Department of Earth Sciences "Ardito Desio", University of Milano, Italy

[4]University of Clermont-Ferrand, France

[5]University of Savoie-Mont Blanc, France

[6]Reykjavik Energy, Bæjarháls 1, 110 Reykjavík, Iceland

[7]Carbfix, Bæjarháls 1, 110 Reykjavík, Iceland

Keywords: hydrogen sulfur, pyrite, geothermal, geo-electrical monitoring, electromagnetics

ABSTRACT

Hydrogen Sulphur (H_2S) is an undesired by-product of geothermal energy exploitation. Previous studies show that H_2S can be injected into the subsurface, where the interaction between injected H_2S-enriched fluids and basaltic formations results in the precipitation of pyrite and other minerals such as smectite. Laboratory measurements and field investigations have shown that the formation of pyrite and smectite can be characterized by their resistivity and induced polarization (IP) signals and detected in volcanic rocks using geo-electric methods. In connection with a test injection of H_2S into shallow 200-500 m wells at the Nesjavellir geothermal site, which is meant to start in December 2020, we are investigating the capabilities of different geophysical methods to image H_2S sequestration in basalts. The methods applied are: transient electromagnetic (TEM) soundings, self-potential (SP), surface DC/IP measurement (also known as electrical resistivity tomography, ERT) and borehole logging of DC/IP. In this study, we present the set-up used for data acquisition of two baseline measurements, which were carried out prior to the H_2S injections. We show that the geophysical methods are efficient tools for establishing the baseline and determine the natural variability of the subsurface resistivity. We discuss the limits and advantages of the different methods and how the set-up has been changed between the two baseline measurements in order to improve the depth of investigation and the resolution of the final models. The TEM, SP, and surface DC/IP results from the Nesjavellir geothermal site show a good compliance between the methods and an insignificant variation in the baseline resistivity from 2019 to 2020. The high resolution and deeper levels reached by DC/IP borehole logging provide complementary information on the resistivity distribution around the wells. Preliminary signal processing of time-domain IP data provides three decades of smooth, exponentially decaying, chargeability curves, which can be fitted with IP models. Upon post-H_2S injection monitoring, the retrieved IP parameters should allow further interpretation in terms of quantity and grain size of newly formed pyrite, by applying established petrophysical relationships.

1. INTRODUCTION

Hydrogen sulphur (H_2S) is an undesired by-product of geothermal energy exploitation due to its corrosive nature, odor and toxicity at high concentrations (Sigfússon *et al.*, 2018, Júlíusson *et al.*, 2015). During the winter 2020/2021, the geothermal power company ON Power, a subsidiary of Reykjavik Energy, will start a small-scale injection of H_2S and CO_2 dissolved in seal water from vacuum pumps at Nesjavellir, South-West Iceland. This small-scale injection will be done alongside larger-scale injection of separated geothermal fluid from the power plant that is part of normal operations. The injection takes place in eight shallow wells whose depth ranges from 311 m to 660 m depth. The GEMGAS project (Geo-Electrical Monitoring of H_2S Gas Sequestration) uses this opportunity to achieve a proof of the concept that geo-electrical measurements can be used to monitor the sequestration of H_2S in basaltic rocks.

Interaction between H_2S-enriched fluids and basalts easily leads to the formation of pyrite (FeS_2), dissolution of iron-oxides (Fe-ox) crystallized from the magma, and the formation of smectite (Stefánsson *et al.*, 2011). At Hellisheiði (South-West Iceland), experiments involving injection of CO_2 and H_2S dissolved in water and monitoring of the chemical composition and mineral saturation indicated that H_2S is rapidly mineralized (e.g. Snæbjörnsdóttir *et al.*, 2017). Since then, industrial scale injection has been on-going in the field, with about 5000 tons of H_2S injected annually (Sigfússon *et al.*, 2018). Chemical monitoring, using wells in the vicinity of the injection, indicate that H_2S is mineralized rapidly. However, physical confirmation and further knowledge on where and in what patterns the pyrite is forming are still lacking. For this purpose, imaging the sequestration processes from the surface would be valuable in particular with regards to optimization of future injections, but also in order to increase the public awareness and acceptance of both CO_2 and H_2S sequestration in basalts.

Petrophysical laboratory measurements indicate that the presence of pyrite can be detected in altered volcanic rocks, and quantified to some extent, by measuring two electrical parameters: the bulk resistivity and the maximum phase angle (MPA) (Lévy *et al.*, 2019a). The bulk resistivity describes the amplitude of the electric conduction phenomenon in rocks, which is in particular enhanced by the presence of smectite, as well as high porosity, salinity and temperature (Flóvenz *et al.*, 2005, Kristinsdóttir *et al.*, 2010, Lévy *et al.*, 2018, Waxman and Smits, 1968). The MPA describes the amplitude of the polarization phenomenon in rocks, which is particularly strong at interfaces between fluid and semi-conductors, such as pyrite or magnetite (Bücker *et al.*, 2018, Gurin *et al.*, 2015, Abdulsamad *et al.*, 2017). The MPA is obtained through complex resistivity measurements, also called Induced Polarization (IP),

which in the time domain requires recording the full transient voltage decay, also called relaxation response (often measured in the current off-time) and not only the steady state, Direct Current (DC), voltage. Geo-electrical investigations at Krafla, in North-East Iceland, confirm that the signal of naturally present pyrite, smectite and magnetite can be picked up, including a differentiation between them, down to 200 m depth, based on joint inversions of the bulk resistivity and MPA from surface DC/IP measurements (Lévy *et al.*, 2019b). These studies thus indicate that the bulk resistivity and the MPA distributions imaged by geophysical measurements are appropriate parameters to describe the changes in mineralogy associated with H_2S sequestration.

The goal of this project is to explore the capabilities and limits of several geophysical methods for imaging the underground changes associated with H_2S injection and to increase the understanding of the processes at play. Five geophysical methods are investigated in the GEMGAS project: transient electromagnetic (TEM) methods, self-potential (SP), surface DC/IP measurement (also known as electrical resistivity tomography, ERT), casing-to-surface DC/IP, and borehole logging of DC/IP. At the time of writing, injection of H_2S has not yet taken place at the Nesjavellir site. Here, we present how the baseline signal was established throughout 2 years of measurements and progressive improvements of the geophysical methods, in order to adjust them to context-specific challenges. First post-injection measurements are planned for January 2021, in order to see if changes in the resistivity or polarization can be observed shortly after injection.

2. GEOPHYSICAL METHODS

An overview of the area, including roads, boreholes and buried infrastructure, is presented Figure 1 together with the surface geophysical setup used for measurement in 2019 and 2020. Strengths and limits of the five methods used in the GEMGAS project are summarized in Table 1 in terms of the depth of investigation (DOI), the vertical resolution, and the area coverage of each of the methods. It should be noted that the surface DC/IP measurements have varying DOI depending on the power available for current injection and the electrode combinations. The control of these setting also depends on the instrument used for the data acquisition. In the GEMGAS project two different types of instruments were considered and a comparison of their resolution capabilities is presented in Figure 2. It should also be noted that the casing-to-surface DC/IP method is still under development and the method is therefore not described further.

In September 2019, the first measurements were carried out to establish a baseline before the H_2S injection. The results were then used to optimize the different instruments and measurement setups, and with the implemented optimizations, a second baseline was measured in July 2020. The following section presents how the four geophysical methods were used in 2019 and 2020 (all methods besides casing-to-surface DC/IP).

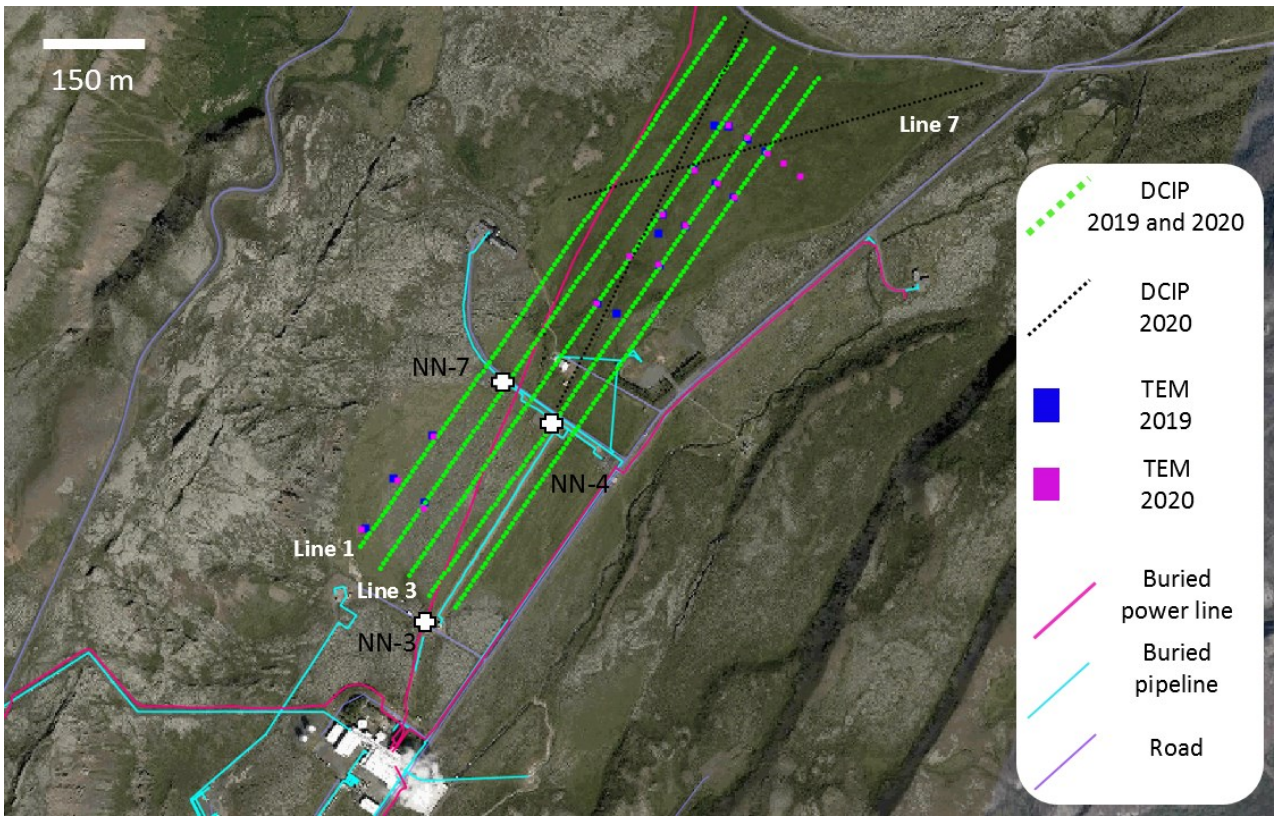

Figure 1: Aerial map of Nesjavellir valley where the geophysical investigations take place. Boreholes NN-3, NN-4 and NN-7 (marked with a white cross) are used for borehole logging acquisition. The position of DC/IP lines no. 1, 3 and 7 are indicated on the figure to allow further referencing of DC/IP inversion results.

Table 1: Comparison of the five geophysical methods used in the GEMGAS project.

	Depth of investigation	Vertical resolution	Surface area coverage	Technology	Limits
TEM	100s m	10s m (depending on depth)	unlimited	In use	Coupling
Self-potential	-	-	unlimited	In use	Ambiguous
Surface DC/IP	10s -100s m (depending on set-up)	1-10s m (depending on depth)	unlimited	In use	Signal level
Casing-to-surface DC/IP	100s m (depending on the depth of the borehole)	10-100s m	Limitations due to placement of borehole	In development	Modelling
Logging DC/IP	100s m - kms (depending on the depth of the borehole)	0.5 m	Local: limited to the borehole	In development	Casing, logger memory and band-width

2.1 TEM

Despite the presence of infrastructure, a good coverage of the area with TEM data has been achieved. Usually two types of electromagnetic coupling can be observed in TEM data: capacitive coupling from buried cable along the road and inductive coupling from fences forming a circular circuit. Close to the power line and to the main roads, a few of the 2019 TEM soundings were highly influenced by the coupling, so these sounding where not reproduced in 2020.

Two different ground-based TEM system were applied for the baseline measurement in 2019: *WalkTEM* with a 50x50 m^2 transmitter coil (from Aarhus University, Denmark) and *ProTEM* with a 100x100 m^2 transmitter coil (from ÍSOR, Iceland). Due to the lower transmitter moment, *WalkTEM* data goes into noise at the late times of the signal. Consequently, the *ProTEM* provide one extra time decade of data at late times, thus gaining a deeper DOI. However, fewer soundings can be made with the bigger *ProTEM* coil in the area, due to a higher influence of electromagnetic coupling. Overall both systems are complementary and yield similar results. Only the only *WalkTEM* system was used to repeat the baseline measurements in 2020.

The TEM inversion results presented in this study where carried out with *AarhusInv* (Auken *et al.*, 2014), using a 3D voxel model mesh combined with 1D forward responses. The inversion is carried out as a time-lapse, where the 2019 and 2020 datasets are inverted simultaneously with constrains (regularizations) between the resistivity values and the resistivity gradients in the two models.

2.2 Self-potential (SP)

Self-potential measurements were carried out with non-polarizable Cu/Cu(SO4) electrodes, along five profiles corresponding to the DC/IP profiles repeated in 2019 and 2020 (see Figure 1). Acquisitions consists of voltage measurements between a reference point and other points covering the area. Since acquisition took place over 2-3 days, temporary references were used and later reduced to a single reference to compute the corrected SP value. The dataset was further interpolated to produced horizontal SP maps presented here.

2.3 Surface DC/IP

2.1.1 Theoretical comparison of two different instruments

A comparison between expected resolution and depth of investigation (DOI) of three different configurations is presented in Figure 2: (i) dipole-dipole array where the voltage and current dipoles do not overlap (DP-DP), (ii) pole-dipole, which is similar to DP-DP with one of the current electrodes far away (P-DP) and (iii) gradient array, which is a type of "nested" array, i.e. where the voltage dipole is between the current electrodes, that allows multiple voltage acquisitions for the same current injection (Loke, 2004). Theoretically, the DOI of P-DP is the deepest (see Figure 2) but noise levels also tend to be higher with this configuration, while gradient configuration usually has the best signal level, especially for IP data. Two different data acquisition instruments are considered in this synthetic analysis: *IRIS Syscal fullwavers* "*FW*" and *ABEM Terrameter*. The major difference is that *FW* allow injecting up to 5 kW (5 A at 1000 V) thanks to a complete separation between the transmitting and the receiving circuits. The increased signal level thanks to the high current injected allows using configurations that would result in pure noise with the *ABEM* system (where a maximum of 500 mA at 600 V can be injected in surface electrodes, in the most optimal cases), such as the P-DP with a current electrode at 4 km distance from the other current electrode. It is clear from Figure 2 that measurements with *FW* have a better resolution below the modelled conductor. However, in order to reach these depths, larger spacing between electrodes are used (typically 50 m between receiver-dipoles), resulting in a loss of resolution, compared to a typical *ABEM* profile with 10 m spacing between electrodes. Ideally, combining these two methods would allow a high DOI while keeping a good vertical resolution. Due to logistical issues, only the *ABEM* system could be used to establish the two baselines.

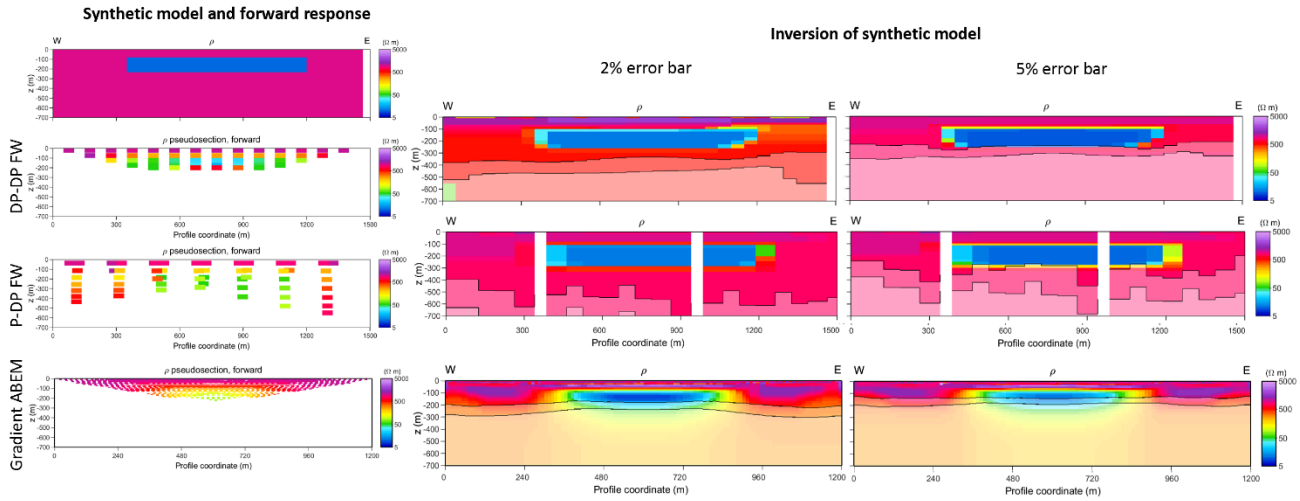

Figure 2: Synthetic analysis of Electrical Resistivity Tomography with 3 different configurations (3 bottom rows) and 2 different data error levels (2 right-most columns) for a resistivity model corresponding to a simplification of the inversion model obtained with measurements in 2019 (upper left frame). Black lines indicate the inferred depth of investigations, with conservative and standard thresholds for sensitivity. The transect simulated here corresponds to the expected average response along each of the five green profiles on Figure 1. Note that the profile coordinate (x-axis) is different for the FW (DP-DP and P-DP) and ABEM (gradient) instruments.

2.1.2 DC/IP acquisition and inversion

In 2019, a coarse resolution DC/IP set-up with 40 m spacing between neighboring electrodes and a total of 1.4 km layout was intended to yield around 400 m DOI. To further increase the DOI, an extension to 1.8 km was attempted through the addition of remote electrodes. However, an accumulation of technical issues resulted in a dataset with large error bars, leading to high model misfits and limited DOI. In 2020, we changed strategy and focused on improving the signal level. We carried out the same profiles with 10 m spacing instead, using cables that allowed injecting up to 600 V (instead of 300 V for the cables used in 2019). Figure 1 shows the 5 lines used in 2019 and 2020 (green), as well as two additional lines used in 2020 (black) where minimum influence of buried pipelines and power lines could be achieved.

In both 2019 and 2020, full waveforms DC/IP data were recorded with the *ABEM Terrameter* instrument, using a 100% duty cycle with 8-seconds pulses and a sampling rate of 3750 Hz. In 2020, up to 500 mA could be injected thanks to relatively low contact resistances (mostly below 1 kΩ). However, the acquired time-domain IP data are strongly affected by 50 Hz noise coming out from the power line. A signal processing algorithm was applied to the full waveform data in order to remove the 50 Hz noise, as presented by Olsson *et al.* (2016). The software *AarhusInv* (Auken *et al.*, 2014) was hereafter used for inversion of the DC/IP data. The 2D DC inversion results presented below, were computed following Fiandaca *et al.* (2013). In most cases, 2D inversions are sufficient to resolve layered structures in the underground, however, if the structures are explicitly 3D or high conductivity contrasts are present, the 2D inversion may not be able to fit the data. For this reason, we are currently working on inverting all the DC profiles together in 3D following Madsen *et al.* (2020). A problem often associated with full 3D inversion is the large demand on computational power (time and memory usage) given the large number of data and model cells. In this study, we therefore also present preliminary results of a 2D-3D hybrid DC inversion (referred to as 2.5D), where a 3D forward response is used in combination with a 2D model mesh. With this method, more accurate forward responses can be obtained without increasing the computation time significantly.

2.4 Logging DC/IP

We use an innovative borehole logging tool, the *QL40-IP* probe manufactured by *ALT*, to measure normal resistivity log and corresponding time-domain IP response, which is possible thanks to recording of full waveform voltages. Traditional applications of the tool, e.g. in the mining industry, are typically fulfilled with 250 or 500 msec current injections. Based on previous studies, we considered that current injections should last minimum 2 seconds, in order to retrieve the expected disseminated pyrite signal upon H_2S injection. Due to the fixed number of 420 sample points in the whole cycle (T_{on}+ - T_{off} – T_{on}- - T_{off}), the sampling rate for 2-seconds and 500 msec current injection were 50 Hz and 200 Hz, respectively. Measurements with these acquisition settings were carried out in NN4 in December 2019. Strong 50 Hz power line noise was identified in the 500 msec dataset (recorded with 200 Hz sampling rate). This noise, which was aliased in the 2-second dataset, is attributed to the presence of the 132 kV buried power line connected to the power plant. Further investigations showed that the power line frequency is not constant within 2 seconds but oscillates between 50.2 and 50.4 Hz. Therefore, much higher sampling rate than 50 Hz was necessary to model the noise and remove it before data analysis.

Given the limitations of the initial tool, the probe manufacturer *ALT* built a new processing board in the summer 2020, in order to fulfill our need for high sampling rate and 2-second injections. The new tool is now able to record 4000 sample points in the full cycle, which allows cycles with 2-second injections and 451 Hz sampling rate. Measurements with the new probe, carried out in September 2020, are presented in this paper.

3. RESULTS

Based on the baseline results from the first measurement campaign in 2019, a set of modifications to the field setup was implemented before the 2020 campaign was carried out. The new baseline results show, in particular, significant improvements in surface DC/IP and IP logging data quality. In addition, the comparison between the two baselines provides an estimate of the natural variability in the signal before injection, especially for TEM and SP data. In the following section, we present (i) TEM time-lapse inversions in 2019 and 2020 and (ii) self-potential horizontal maps in 2019 and 2020, further compared to (iii) horizontal resistivity map from DC inversion in 2020, that allow identifying a common artefact along the direction of the buried power line. We then evaluate the consistency of (iv) DC and TEM resistivity baseline models in 2020 and discuss results from (v) 2.5D DC inversion. Finally we present (vi) the borehole logging baseline for DC and IP in three wells.

3.1 TEM time-lapse

Based on the 2019 and 2020 WalkTEM data, a time-lapse TEM inversion was carried out with the two datasets to evaluate any natural variability in the signal. The inversion converges with a very satisfactory misfit and shows similar 3D models from 2019 and 2020, with the conductive layer at the bottom being slightly more conductive in 2020 (Figure 3). The conductivity increase can be explained by the continuous injection of warm water between the two field campaigns.

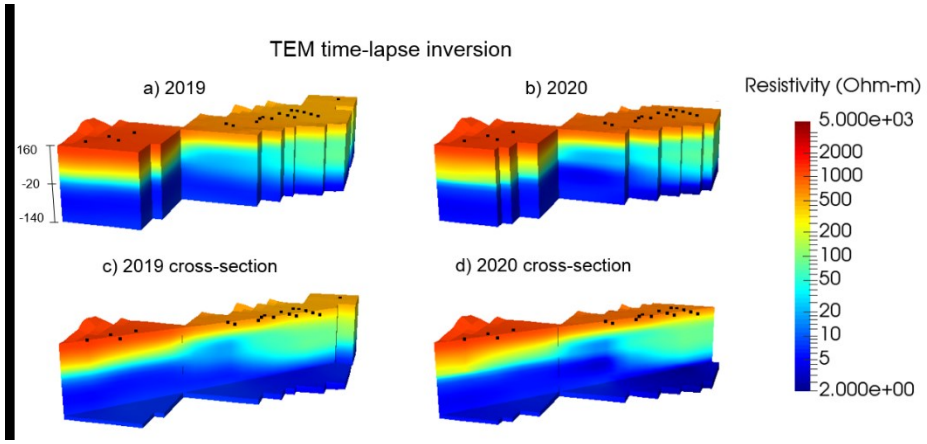

Figure 3: TEM inversion models from 2019 and 2020 obtained with time-lapse regularization. Full model volumes are presented in the top frames, while cross-sections are shown underneath to show the changes inside the volume. The bottom of the volumes are also displayed in the lower frames to clearly mark where the cross-section is cut.

3.2 Comparison of SP in 2019 and 2020

The SP measurements, carried out at similar locations in 2019 and 2020, show very consistent structures (Figure 4). The large anomaly running NW-SE is overlapping the tracks of the buried 132 kV. Subsurface grounding of the power line might explain the constant, stable, negative voltage measured closed to the tracks. Small variations from 2019 to 2020 around the three wells NN-4, NN-3 and NN-7 is likely due to different injection activity in these wells at the time of the measurements. The differential map shows that (i) the NW-SE infrastructure artefact is not significantly changing from year to year and (ii) small differences in fluid flow, temperature and composition can be detected with the SP methods.

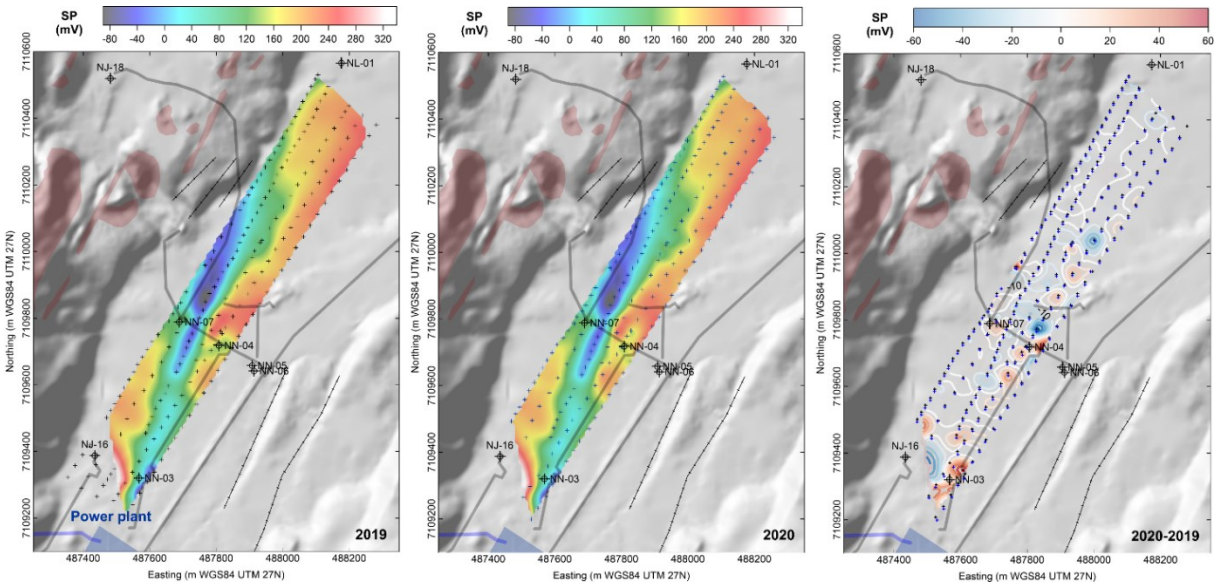

Figure 4: Self-potential maps from 2019 and 2020, together with the difference (2020-2019). These maps represent the SP signal measured with surface electrodes, which corresponds to an integration of the signal over depth.

3.3 Artefacts in DC and SP

The 2020 DC data have been processed and inverted in 2D and, as expected, show much higher resolution and quality, with a significantly reduced data misfit, compared to the 2019 profiles. Consequently, the DOI was increased (down to 300-350 m) although a shorter electrode spread was used. Thanks to the improved resolution and signal/noise ratio, a new source of systematic noise appears clearly: effect of buried power line and unknown infrastructure connected to the central farmhouse, on both DC and IP data (Figure 5). This effect is also seen in SP data (Figure 4).

The resistivity drop along the power line, associated to negative SP anomaly can be interpreted as the result of power line grounding in the subsurface. It is likely that the grounding creates constant currents in the ground that are picked up by our self-potential measurements. If this constant negative voltage is also picked up by our surface voltage measurements during the DCIP acquisition, it could explain an apparent decrease of resistivity ("artificial" decrease of total voltage measured and thus resistance).

The IP data quality is significantly better in 2020 and the chargeability curves affected by the buried infrastructures (power line, pipeline, house foundations) can be better discriminated from non-affected curves. The 2019 data did not allow any meaningful IP inversion on the other hand. Work on surface IP data is still on-going and only DC inversions are presented in the rest of the study.

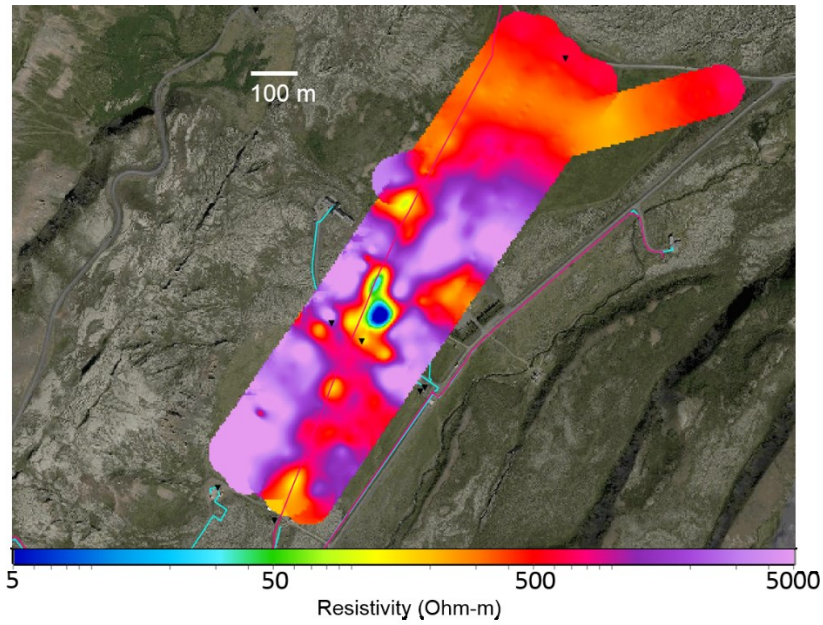

Figure 5: DC resistivity horizontal section at 135 m elevation (close to the surface) created from kriging of 2D inversion results of the seven DC/IP surface profiles (see Figure 1 for the profile positions). The resistivity section shows shallow artefact related to the house foundation and 132 kV buried power line.

3.4 Comparison of DC and TEM

Despite the shallow infrastructure artefacts, reliable 2D DC inversions are obtained at all seven profiles with 2020 data. Three profiles are presented in Figure 6. The 2D DC resistivity models are further compared to 1D TEM resistivity models, represented by vertical bars in Figure 6. Given the overall consistency between 2D DC and 1D TEM inversion, joint inversion of DC and TEM might allow obtaining a unique resistivity model, well resolved at the surface by DC data and defining precisely the depth to the main conductor thanks to TEM.

Figure 7 shows preliminary 2.5D inversion results of profile 1. The inversion time, final misfit, and retrieved resistivity model are similar to the 2D inversion results. At the South-West (left) side of the profile, however, the low resistivity volume resolved by the 2D inversion is not seen in 2.5D. This can be due to limited resolution at the edge of the profile or different data fits to 3D effects. To draw further conclusions, more synthetic tests using the 2.5D approach should be considered including studies of 3D effects and sensitivity patterns.

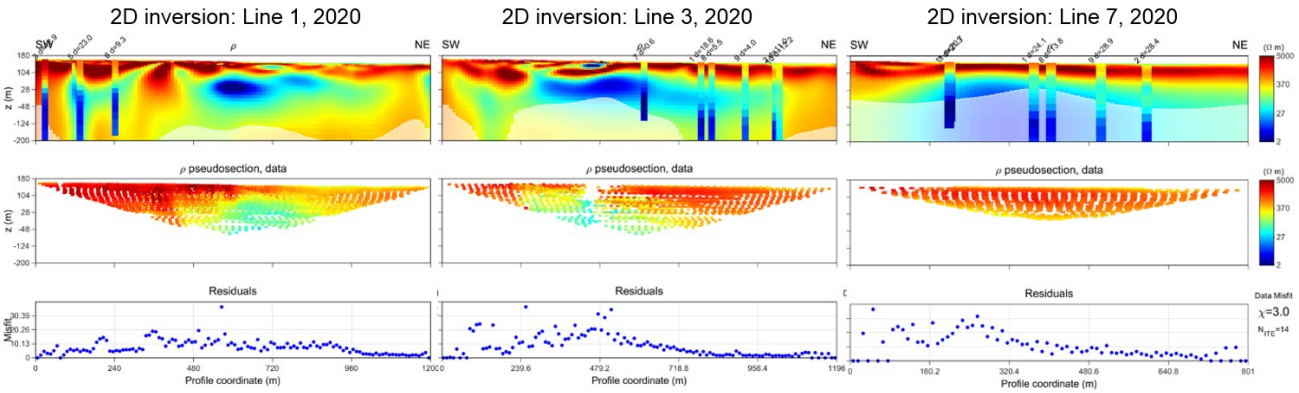

Figure 6: 2D inversion results of DC data in 2020 at profiles 1, 3 and 7 (from left to right), overlapped by 1D inversion of TEM soundings at locations close to the respective profiles. Transparency indicates models below depth of investigation. The location of the three profiles is indicated in Figure 1.

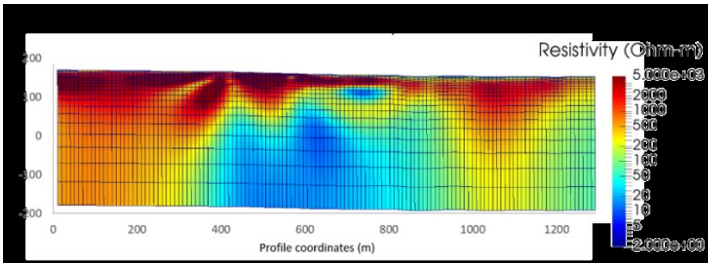

Figure 7: 2.5D inversion results of DC data from 2020 at profile 1. In the inversion, the 3D forward response is computed in a 3D mesh and the model update is done in a 2D structured mesh as seen in the figure.

Overall, a large low-resistivity anomaly is observed at 80m depth (100m elevation) and seems to extend downwards to 230m depth (-50m elevation). Since this anomaly is new, compared to TEM and Schlumberger soundings carried out in the area in 1986 (Arnason *et al.*, 1986), it is attributed to the disposal of hot waste water from the power plant that has been on-going in the subsurface since 1990. A similar up-doming low-resistivity anomaly has been identified in a recent electromagnetic survey (including magneto-telluric and *ProTEM* 200x200m), although its contours cannot be delineated accurately by the coarser resolution inherent to magnetotelluric and *ProTEM* surveys.

Temperature monitoring in the area indicate that subsurface temperature does not exceed 70°C above 500 m depth, therefore a rise in temperature alone cannot explain resistivity values below 5 Ωm (Lévy et al., 2019b). The low-resistivity body is thus interpreted by the progressive formation of smectite triggered by an increase of water temperature due to geothermal fluid disposal in the shallow groundwater system.

Maximum depth of investigation (DOI) of 400m was achieved for DC in profile 1 (Figure 6), and in particular sufficient data sensitivity was available below the main conductor in this profile. The best data quality was obtained in this profile, thanks to large current injection, repeated measurements and limited influence of infrastructure effects. For other DC profiles, the DOI is limited at the lateral position of the main conductive anomaly. Further data processing might help improve the DOI.

These results illustrate the effects of hot water injection on the upper part of the geothermal reservoir. They also indicate that monitoring pyrite formation by surface DC/IP measurements will be challenging, because high-conductivity formations, whether due to smectite or conductive pore water, tend to reduce the strength of induced polarization signals due to the low voltage measured (Lévy *et al.*, 2019b, Lévy *et al.*, 2019c).

3.5 Logging DC/IP

Average resistivity in NN-4 and NN-7 is around 20-30 Ωm, with the whole depth range of logging data being below the main conductor observed in DC/IP profiles (Figure 8). The 2D and 2.5D inversions of Line 1 also shows average resistivity values around 30 below the conductor (Figures 6 and 7). NN-3 is located more south, compared to NN-4 and NN-7, and indicates overall more resistive structures in the logging results. This is also consistent with the higher resistivity observed in the SW part of profiles 1 and 3 in Figures 6 and 7. The three logging datasets extend the image of resistivity distribution down to 550 m at discrete locations. Comparison of future logging campaigns to this baseline will allow monitoring accurately resistivity changes related to the change in composition of injected fluid.

Development of an appropriate signal processing strategy for this original time-domain IP dataset is still on-going, including power line noise modelling and log-gating. The goal is to optimize the signal-to-noise ratio and maintain three decades of signal for the chargeability curves. Typical algorithms for signal processing TDIP data usually rely on much higher sampling rates, e.g. 3750 Hz for ABEM Terrameter data (Olsson *et al.*, 2016), so that algorithms need to be adjusted to this specific case. Preliminary results show excellent chargeability data quality, from 0.003 to 2 seconds, in the three wells (Figure 8). Smooth changes as a function of depth are

observed in the three wells, with all decays following a similar shape in a relatively narrow range. Thanks to the high-resolution high-quality chargeability decays, highlighted by these preliminary results, localized and subtle changes in the IP response of the formation upon pyrite precipitation should be detectable. Moreover, the three decades of signal recovered after signal processing should allow a decent decomposition of the signal in frequency-domain, i.e. an identification of the main peak frequencies, which can be interpreted in terms of grain size of newly formed pyrite.

Future data analysis steps include applying IP-decay models to the processed chargeability curves, such as Cole-Cole, relaxation time distribution or simple stretched exponential function (Fiandaca *et al.*, 2012, Nordsiek and Weller, 2008). Furthermore, one-dimensional inversion of resistivity and IP data will be attempted to obtain a more realistic representation of the subsurface resistivity and polarizability structure.

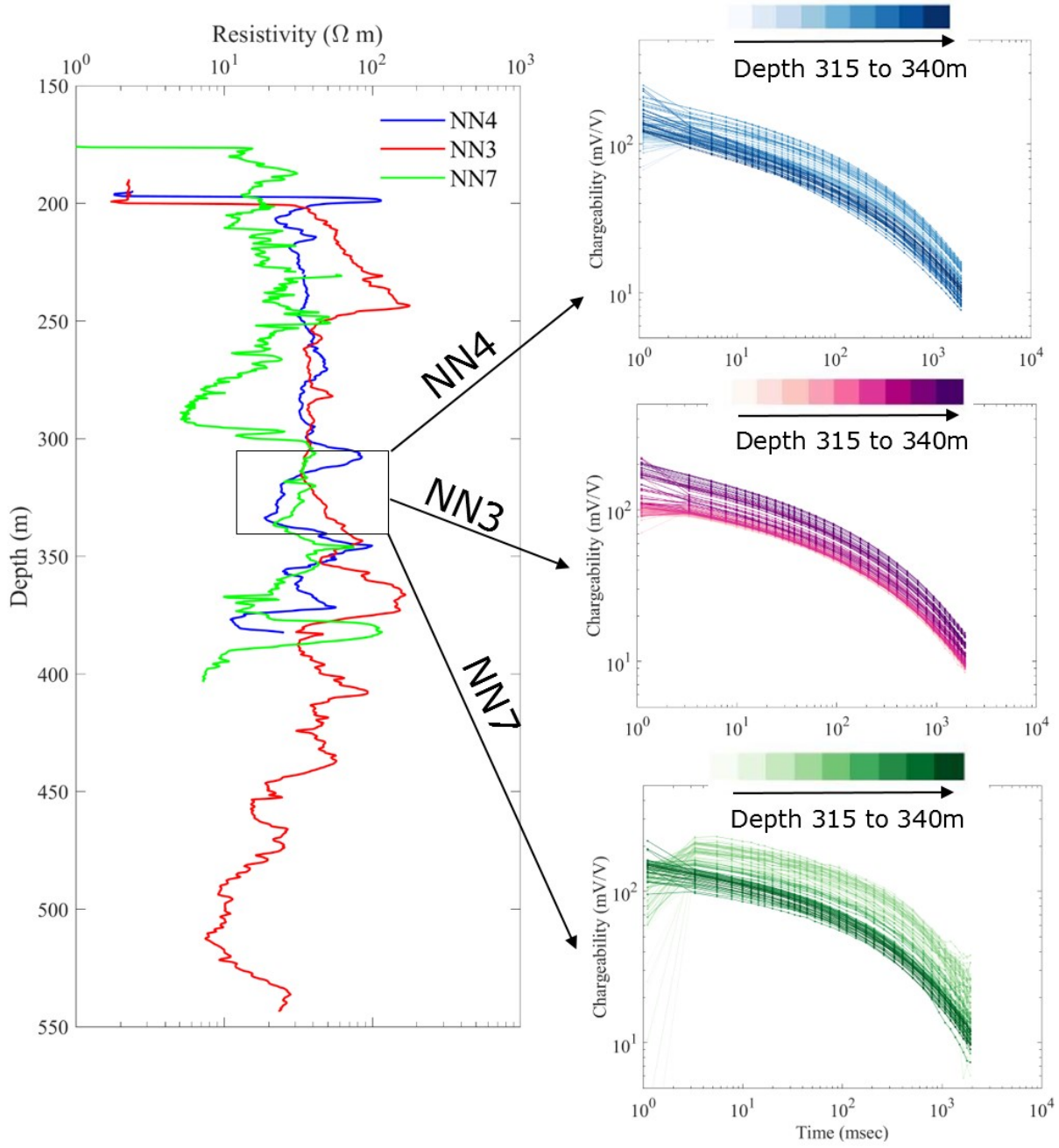

Figure 8: Left panel: resistivity logs in the three wells NN3, NN4 and NN7. Right panels: Chargeability decays in each well, computed for 100 electrode configurations, with focus depth in the rectangle marked on left panel. All data measured with the QL-40 IP probe in September 2020 (before start of H2S injection). Note that NN-7 is drilled directionally (not vertically) and depths are corrected according to the dipping angle.

4. CONCLUSIONS

In this study, we investigated the capabilities and limits of four geophysical methods with regards to monitoring the injection of H_2S in the shallow part of Nesjavellir geothermal reservoir.

We clearly identified a low-resistivity anomaly between 80 and 230m depth (possibly deeper), with a good agreement between 2D DC and 1D TEM models in terms of depth-to-conductor and overall resistivity distribution. The important resistivity contrast and anomaly shape is further confirmed by 2.5D DC inversion. This anomaly, mostly pronounced at the center of Nesjavellir valley, is interpreted as a probable presence of smectite, precipitated in the basalts in reaction to the disposal of geothermal waste water, which is on-going since the start of the power plant in 1990. The agreement between DC and TEM, as well as the consistency between TEM models from 2019 and 2020, allows establishing a reliable resistivity baseline model, well-resolved near the surface by DC and reaching 400 m in most places thanks to TEM and DC combined.

However, this unexpected low-resistivity structure makes future monitoring based on surface data challenging for two reasons. First, the depth of investigation of geo-electrical and electromagnetic methods is often limited by the presence of thick conductors at depth, because only strong current lines can penetrate deeper. Deeper DOI for DC measurements could theoretically be achieved with modern systems such as the IRIS Syscal fullwavers, which allow sending significantly higher currents, as illustrated by a simple synthetic analysis. Using such an instrument is associated with complex logistics and safety matters, which have not yet been overcome in the life of the GEMGAS project. Future work includes more advanced synthetic analyses based on different scenarios for pyrite precipitations (big cluster or disseminated particles) and using predictions from reactive transport models.

Self-potential data measured in 2019 and 2020 show an overall very stable baseline with subtle differences localized around the injection wells and attributed to different injection activity between the two years. The overall stability of the signal is promising for monitoring the injection of low pH H_2S-enriched fluids at high flow rate. Self-potential could be used as a regular monitoring tool, thanks to the ease-of-use of the method.

Significant effects of buried infrastructure (in particular power line and house foundations) are observed in our data and inversion results. In the case of DC data, the infrastructure results in a shallow, localized structure, which is recovered by the inversion and can be separated from what is considered to be the "geological" response. In the case of self-potential data, only time-lapse differences can be interpreted due to infrastructure effects. The area coverage by TEM soundings is also limited by the presence of fences, roads and buried power line, which give rise to inductive coupling whenever the transmitter coil is too close to these structures.

The greatest data quality, in particular for time-domain IP, is achieved by borehole logging in three injection wells. The preliminary results presented here illustrate the potential of this tool for regular monitoring of pyrite precipitation upon H2S injection with high vertical resolution, in the vicinity of the wells (maximum one meter away from the well). Future work includes fitting the chargeability curves with IP models and one-dimensional inversion.

6. ACKNOWLEDGMENT

The authors warmly thank the international team involved in challenging field work in 2019 and 2020: Halldór Ö. Stefánsson, Halldór Ingólfsson, Jón Einar Jónsson, Mohammed Rizwan Asif, Rune Kraghede, Thierry Souriot and Benoit Gibert. We also thank Jean Vandemeulebrouck and Philippe Labazuy for valuable discussion and equipment availability in 2019, as well as Bruno Legros for tremendous assistance in relation to the QL40-IP tool use and improvements. In addition, Jakob Juul Larsen is thanked for very appreciated help with signal processing of logging IP data. A large team of people at ÍSOR, Reykjavik Energy and Aarhus University have ensured, and continue to ensure that the field work is carried out in appropriate conditions, thanks to good coordination and logistics. We thank in particular Ásdís Benediktsdóttir, Vala Hjörleifsdóttir, Íris E. Einarsdóttir, Bjarni S.Gunnarsson and Jesper B. Pedersen. The GEMGAS project received funding from the Technological Innovation Fund, *Tæknibróunarsjóður*, at the Icelandic Research Agency, *Rannsóknamiðstöð Íslands*. Additional developments by the R&D department at Advanced Logic Technology, *ALT*, allowed essential improvements of the QL40-IP logging tool for this study.

REFERENCES

Abdulsamad, F., Florsch, N. & Camerlynck, C., 2017. Spectral induced polarization in a sandy medium containing semiconductor materials: experimental results and numerical modelling of the polarization mechanism, *Near Surface Geophysics,* 15**,** 669-683.

Arnason, K., Haraldsson, G.I., Johnsen, G.V., Thorbergsson, G., Hersir, G.P., Saemundsson, K., Georgsson, L.S., Rognvaldsson, S.T. & Snorrason, S.P., 1986. Nesjavellir-Olkelduhhals, Surface Investigations (report in Icelandic)Orkustofnun, Reykjavik.

Auken, E., Christiansen, A.V., Kirkegaard, C., Fiandaca, G., Schamper, C., Behroozmand, A.A., Binley, A., Nielsen, E., Effersø, F., Christensen, N.B. & others, 2014. An overview of a highly versatile forward and stable inverse algorithm for airborne, ground-based and borehole electromagnetic and electric data, *Exploration Geophysics,* 46**,** 223-235.

Bücker, M., Flores Orozco, A. & Kemna, A., 2018. Electro-chemical polarization around metallic particles--Part 1: The role of diffuse-layer and volume-diffusion relaxation, *Geophysics,* 83**,** 1-53.

Fiandaca, G., Auken, E., Gazoty, A. & Christiansen, A.V., 2012. Time-domain induced polarization: Full-decay forward modeling and 1D laterally constrained inversion of Cole-Cole parameters, *Geophysics,* 77**,** E213-E225.

Fiandaca, G., Ramm, J., Binley, A., Gazoty, A., Christiansen, A.V. & Auken, E., 2013. Resolving spectral information from time domain induced polarization data through 2-D inversion, *Geophysical Journal International,* 192**,** 631-646.

Flóvenz, O.G., Spangenberg, E., Kulenkampf, J., Árnason, K., Karlsdóttir, R. & Huenges, E., 2005. The role of electrical interface conduction in geothermal exploration. *in Proceedings of World Geothermal Congress 2005*.

Gurin, G., Titov, K., Ilyin, Y. & Tarasov, A., 2015. Induced polarization of disseminated electronically conductive minerals: a semi-empirical model, *Geophysical Journal International,* 200**,** 1555-1565.

Júlíusson, B.M., Gunnarsson, I., Matthíasdóttir, K.V., Markússon, S.H., Bjarnason, B., Sveinsson, O.G., Gíslason, T. & Thorsteinsson, H.H., 2015. Tackling the challenge of H2S emissions.

Kristinsdóttir, L.n.H., Flóvenz, Ó.G., Árnason, K., Bruhn, D., Milsch, H., Spangenberg, E. & Kulenkampff, J., 2010. Electrical conductivity and P-wave velocity in rock samples from high-temperature Icelandic geothermal fields, *Geothermics,* 39**,** 94-105.

Loke, M.H., 2004. Tutorial: 2-D and 3-D electrical imaging surveys.

Lévy, L., Gibert, B., Sigmundsson, F., Flóvenz, Ó.G., Hersir, G.P., Briole, P. & Pezard, P.A., 2018. The role of smectites in the electrical conductivity of active hydrothermal systems: electrical properties of core samples from Krafla volcano, Iceland, *Geophysical Journal International,* 215**,** 1558-1582.

Lévy, L., Gibert, B., Sigmundsson, F., Parat, F., Deldicque, D. & Hersir, G.P., 2019a. Tracking magmatic hydrogen sulphur circulations using electrical impedance : complex electrical properties of core samples at the Krafla volcano, Iceland, *Journal of Geophysical Research: Solid Earth*.

Lévy, L., Maurya, P.K., Byrdina, S., Vandemeulebrouck, J., Sigmundsson, F., Árnason, K., Ricci, T., Deldicque, D., Roger, M., Gibert, B. & Labazuy, P., 2019b. Electrical resistivity tomography and time-domain induced polarization field investigations of geothermal areas at Krafla, Iceland: comparison to borehole and laboratory frequency-domain electrical observations, *Geophysical Journal International,* 218**,** 1469-1489.

Lévy, L., Weller, A. & Gibert, B., 2019c. Influence of smectite and salinity on the imaginary and surface conductivity of volcanic rocks, *Near Surface Geophysics,* 17**,** 653-673.

Madsen, L.M., Fiandaca, G. & Auken, E., 2020. 3-D time-domain spectral inversion of resistivity and full-decay induced polarization data—full solution of Poisson's equation and modelling of the current waveform, *Geophysical Journal International,* 223**,** 2101-2116.

Nordsiek, S. & Weller, A., 2008. A new approach to fitting induced-polarization spectra, *Geophysics,* 73**,** F235-F245.

Olsson, P.-I., Fiandaca, G., Larsen, J.J., Dahlin, T. & Auken, E., 2016. Doubling the spectrum of time-domain induced polarization by harmonic de-noising, drift correction, spike removal, tapered gating and data uncertainty estimation, *Geophysical Journal International,* 207**,** 774-784.

Sigfússon, B., Arnarson, M.Þ., Snæbjörnsdóttir, S.Ó., Karlsdóttir, M.R., Aradóttir, E.S. & Gunnarsson, I., 2018. Reducing emissions of carbon dioxide and hydrogen sulphide at Hellisheidi power plant in 2014-2017 and the role of CarbFix in achieving the 2040 Iceland climate goals, *Energy Procedia,* 146**,** 135-145.

Snæbjörnsdóttir, S.Ó., Oelkers, E.H., Mesfin, K., Aradóttir, E.S., Dideriksen, K., Gunnarsson, I., Gunnlaugsson, E., Matter, J.M., Stute, M. & Gislason, S.R., 2017. The chemistry and saturation states of subsurface fluids during the in situ mineralisation of CO 2 and H 2 S at the CarbFix site in SW-Iceland, *International Journal of Greenhouse Gas Control,* 58**,** 87-102.

Stefánsson, A., Arnórsson, S., Gunnarsson, I., Kaasalainen, H. & Gunnlaugsson, E., 2011. The geochemistry and sequestration of H2S into the geothermal system at Hellisheidi, Iceland, *Journal of Volcanology and Geothermal Research,* 202**,** 179-188.

Waxman, M.H. & Smits, L.J.M., 1968. Electrical conductivities in oil-bearing shaly sands, *Soc. Pet. Eng. J.,* 8**,** 107-122.